Atmos. Chem. Phys. Discuss., 10, 13407–13443, 2010
www.atmos-chem-phys-discuss.net/10/13407/2010/
doi:10.5194/acpd-10-13407-2010

Atmospheric Chemistry and Physics Discussions

Characterizing aerosol transport into the Canadian High Arctic using aerosol mass spectrometry and Lagrangian modelling

T. Kuhn[1], **R. Damoah**[2], **A. Bacak**[3], **and J. J. Sloan**[2]

[1]Department of Space Science, Luleå University of Technology, Kiruna, Sweden
[2]Department of Earth and Environmental Sciences, University of Waterloo, Waterloo, ON N2L 3G1, Canada
[3]School of Earth, Atmospheric and Environmental Sciences, The University of Manchester, Williamson Building, Oxford Road, Manchester, M13 9PL, UK

Received: 1 April 2010 – Accepted: 12 May 2010 – Published: 26 May 2010

Correspondence to: J. J. Sloan (sloanj@uwaterloo.ca)

Published by Copernicus Publications on behalf of the European Geosciences Union.

Abstract

We report the analysis of measurements made using an aerosol mass spectrometer (AMS; Aerodyne Research Inc.) that was installed in the Polar Environment Atmospheric Research Laboratory (PEARL) in summer 2006. PEARL is located in the Canadian high Arctic at 610 m above sea level on Ellesmere Island (80° N 86° W). PEARL is unique for its remote location in the Arctic and because most of the time it is situated within the free troposphere. It is therefore well suited as a receptor site to study the long range tropospheric transport of pollutants into the Arctic. Some information about the successful year-round operation of an AMS at a high Arctic site such as PEARL will be reported here, together with design considerations for reliable sampling under harsh low-temperature conditions. Computational fluid dynamics calculations were made to ensure that sample integrity was maintained while sampling air at temperatures that average −40 °C in the winter and can be as low as −55 °C. Selected AMS measurements of aerosol mass concentration, size, and chemical composition recorded during the months of August, September and October 2006 will be reported. During this period, sulfate was at most times the predominant aerosol component with on average 0.115 $\mu g\,m^{-3}$ (detection limit 0.003 $\mu g\,m^{-3}$). The second most abundant component was undifferentiated organic aerosol, with on average 0.11 $\mu g\,m^{-3}$ detection limit (0.04 $\mu g\,m^{-3}$). The nitrate component, which averaged 0.007 $\mu g\,m^{-3}$, was above its detection limit (0.002 $\mu g\,m^{-3}$), whereas the ammonium ion had an apparent average concentration of 0.02 $\mu g\,m^{-3}$, which was approximately equal to its detection limit. A few episodes having increased mass concentrations and lasting from several hours to several days are apparent in the data. These were investigated further using a statistical analysis to determine their common characteristics. High correlations among some of the components arriving during the short term episodes provide evidence for common sources. Lagrangian methods were also used to identify the source regions for some of the episodes. These showed that the source regions for the two selected episodes were located in north-eastern North America and western Siberia. We be-

ACPD

10, 13407–13443, 2010

lieve the former is associated with sulfate emissions from motor vehicles, power plants and heavy industry. The latter coincides with the locations of the largest Russian oil and gas fields. These conclusions show that the Arctic is the destination for significant amounts of pollution from high- and mid-latitude industrial and resource activity.

1 Introduction

The Arctic is a relatively pristine environment, but it is not completely isolated from distant anthropogenic influences. Information about transport of pollution into the Arctic is documented regularly in the reports of the Arctic Monitoring and Assessment Programme (AMAP), which identify the large-scale tropospheric pathways whereby pollutants are brought from low to high latitudes (AMAP, 2003). One of the most dramatic consequences of this pollution, Arctic haze, is associated with the intrusion of polluted air into the Arctic in winter and spring, when anthropogenic sources and the Arctic are within the same (cold) air masses (Heintzenberg, 1989). Related to this, early measurements showed that anthropogenic aerosols from low latitudes are an important component of Arctic contamination (Hoff et al., 1983). Possibly more important are semi-volatile organic pollutants like pesticides which, like the aerosols, have no high latitude sources, yet are found in high concentrations at many Arctic locations (e.g. Bailey et al., 2000; Halsall et al., 1998; Hung et al., 2005; Oehme, 1991; Oehme and Ottar, 1984). The presence of these clearly identifiable contaminants demonstrates the existence of transport pathways for anthropogenic pollutants into the Arctic.

Much work has been done during more than two decades to identify the sources of these materials This effort is made more difficult by recent indications that the predominant locations of emission sources may be changing (Hung et al., 2005; Sirois and Barrie, 1999). Some reports suggest that these originate in regions of Eurasia, but parts of North America have also been indicated for some receptor locations (Halsall et al., 1997; Nyeki et al., 2005; Pacyna, 1995; Polissar et al., 2001; Xie et al., 1999). For these reasons and many others relating to the health of the affected communities,

ACPD
10, 13407–13443, 2010

it is important to continue the efforts to monitor and understand long range transport of pollutants into the Arctic.

Particulate matter (PM) in the smaller size ranges (e.g. PM_1), which is transported over long distances (Saarikoski et al., 2008; Sehili and Lammel, 2007), is a useful tracer for the origins of this material as well as a vector for transport of contaminants (Lammel et al., 2009). Many of the important effects occur at Arctic sunrise when photochemical processes begin after months of darkness. Aerosols also cause important radiative effects in the Arctic. For example, increases in the number and size of sulfate aerosols from photo-oxidation of SO_2 can cause surface cooling by reflecting incoming radiation (Hung et al., 2005; Sirois and Barrie, 1999), whereas aerosols of other sizes and compositions can have warming effects. Thus there is a strong connection between the chemical compositions of aerosols and their radiative effects.

There have been many studies of the chemical compositions of Arctic aerosols (e.g. Covert and Heintzenberg, 1993; Heidam et al., 1993; Heintzenberg and Leck, 1994; Sirois and Barrie, 1999; Staebler et al., 1999), some of which also report particle size information (Barrie et al., 1994; Hillamo et al., 2001; Ricard et al., 2002; Teinilä et al., 2003). Not all studies include organic matter, which is a significant fraction of the aerosol (Heintzenberg, 1989) and studies that do include organics usually focus only on toxics like pesticides (Hung et al., 2005) or selected compounds such as dicarboxylic acids (e.g. Narukawa et al., 2002; Teinilä et al., 2003), thereby omitting most of the organic mass fraction.

Finally, most Arctic measurement sites represented in the data referenced above are at or close to sea level, which is a disadvantage when studying long range transport occurring in the free troposphere. Exceptions to this include the Zeppelin site close to Ny-Ålesund on Svalbard, which at 474 m a.s.l., is located in the free troposphere for much of the time. This site has been used for measurements of aerosol chemical composition in several studies (Heintzenberg and Leck, 1994; Ström et al., 2003; Teinilä et al., 2004). Clearly, it is desirable to have more measurements of aerosol size and composition in the high Arctic. Additionally, the temporal variation of these parameters is

ACPD
10, 13407–13443, 2010

less well characterized than the average values and this is also an extremely important factor to explore.

In the following, we report selected measurements of the temporal variations in aerosol size and composition that were carried out at the Polar Environment Atmospheric Research Laboratory (PEARL) in the Canadian Arctic. Located at 80°02′ N, 86°15′ W at an elevation of 610 m, PEARL is in the free troposphere and thus is ideally suited for studying aerosol transport into the Arctic. The measurements were done using an aerosol mass spectrometer (AMS; Aerodyne Research Inc.) that provides a continuous data record with high temporal resolution. These measurements are the first recorded by an AMS in the Arctic and, to the knowledge of the authors, they represent the first time that ground-based real-time chemical analysis of Arctic aerosols has been attempted. We describe here the sampling site and some design features of the installation that were necessitated by the need to ensure the integrity of the samples under the harsh conditions of the PEARL laboratory. Computational fluid dynamics (CFD) simulations of the inlet system are reported, to verify that particles in the size range that can be detected by the instrument were sampled efficiently. We also report analyses by several methods of episodes relevant for studies of long range transport. Statistical analyses and Lagrangian modelling of these were used to provide information about common sources and geographical locations.

2 Site and installation details

2.1 Polar Environment Atmospheric Laboratory (PEARL)

The PEARL laboratory is a facility of the Canadian Network for the Detection of Atmospheric Change (CANDAC) in the Canadian high Arctic. It is located on Ellesmere Island in Nunavut, Canada, 9 km west from Eureka (79°59′ N, 85°56′ W), which is a Canadian High Arctic Weather Station (HAWS). About two kilometres east of the weather station is the Eureka airport and a small military base. Eureka is 160 km north

ACPD
10, 13407–13443, 2010

of the nearest community (Grise Fjord) and about 150 km south-west of the Canadian Forces Station (CFS) Alert, which is home to a more substantial military presence, as well as another HAWS. The PEARL laboratory is located on top of a 610 m ridge, a few kilometres east of Eureka Sound, which runs North-South, and just north of Slidre Fjord, which runs East-West. The neighbouring hills are at similar or lower altitudes, so the laboratory is located within the free troposphere almost all of the time. These geographical features make PEARL an ideal and unique site for an Arctic observatory.

Between 1993 and 2002, the facility, then called the Arctic Stratospheric Observatory (AStrO), was used by Environment Canada (EC) for (mostly) stratospheric observations. The Arctic atmospheric research program at PEARL was initiated under new funding from the Canada Foundation for Climate and Atmospheric Studies (CFCAS), the Canada Foundation for Innovation (CFI), the Ontario Innovation Trust (OIT), and the Atlantic Innovation Fund (AIF)/Nova Scotia Research Innovation Trust (NSRIT). Several new CANDAC programs made possible by this funding have expanded the research scope into the lower atmosphere. Since summer 2005, PEARL has been operated year-round by CANDAC. One to three operators maintain the facility and oversee the experiments. Electric power for the laboratory is produced in Eureka by a diesel generating plant, which is located away from the prevailing wind direction, so measurements at PEARL are not affected by local pollution sources, another important asset of the laboratory.

2.2 AMS installation

An AMS from Aerodyne Research Inc. (Canagaratna et al., 2007; Jayne et al., 2000; Jimenez et al., 2003) was installed at PEARL in August 2006. The AMS provides near real-time size resolved composition analysis of non-refractory particulate matter in the size range from approximately 80 nm to 700 nm. During operation, particles are aerodynamically focused in a high-vacuum system (Liu et al., 2007) onto a heated surface (temperature ~540 °C) where non-refractory components are thermally vaporised and analysed by electron impact (70 eV) ionization quadrupole mass spectrometry. The

ACPD
10, 13407–13443, 2010

instrument at PEARL (a 215 series AMS) has a particle time of flight (TOF) path of 293 mm and a critical orifice diameter of 0.1 mm, which fixes the inlet flow rate at approximately 1.3 $cm^3\,s^{-1}$ (≈80 $ml\,min^{-1}$).

The AMS is operated at a normal room temperature of approximately 20 °C inside the PEARL laboratory. An air stream of 11 $l\,min^{-1}$ (laboratory temperature and pressure) is sampled through an inlet assembly located about 2.2 m above the roof of the laboratory and flows to the AMS through a 22 mm ID stainless steel inlet pipe, which is approximately 7.2 m long. The flow rate and pipe dimension results in laminar flow with a Reynolds number (Re) of approximately 700. Close to the AMS, the flow is split in three parts: a 1 l/min flow to the AMS and two 5 $l\,min^{-1}$ flows, which can be used to sample total suspended particles (TSP) and PM_1 on filters. (The latter measurements will not be reported here.) The 1 $l\,min^{-1}$ flow is transferred to the inlet of the AMS through a 37 cm long, 5.2 mm ID stainless steel tube at Re≈300. A stainless steel tube approximately 15.5 cm long and 2 mm ID sub-samples the AMS inlet flow rate of 80 $ml\,min^{-1}$ from the core of the 1 $l\,min^{-1}$ flow and delivers it to the critical orifice of the AMS inlet. This sub-sampling is slightly sub-isokinetic; the mean speed in the 2 mm ID sampling tube is approximately half of the mean speed in the 5.2 mm ID tube with the 1 $l\,min^{-1}$ flow. This however, does not present a problem, because the inertia of 1 µm particles is negligible (Stokes' number Stk=0.001 for 1 µm particle with density of water and 2 mm ID sampling tube). Thus the sub-sample of 1 µm and smaller particles is representative of the sample in the 1 l/min flow.

Figure 1 shows a 30° radial section through the inlet assembly on the laboratory roof. The outer surface is an inverted, heated cylindrical cup (120 mm ID), which is insulated on the outside. The cup surrounds the inlet pipe, which is flared slightly at the top to resemble a funnel, with a 38.1 mm diameter top opening that narrows to 25.4 mm at the bottom. Both the funnel and the cover are maintained at a temperature of 20 °C in order to bring the sampled air to room temperature quickly when it enters the inlet. This removes larger ice crystals that might otherwise not evaporate completely before being sampled by the AMS (Staebler et al., 1999). After passing through the inlet assembly,

ACPD
10, 13407–13443, 2010

air enters the inlet pipe, which passes through a 10 cm diameter, 3 m long PVC tube mounted in an insulated hatch in the roof of the room where the AMS is located.

Care was taken to ensure that the sampling system would work properly, even for the lowest (−55 °C) outside temperatures encountered in the winter. The temperature changes caused by bringing the sampled air to the temperature of the AMS inlet could cause buoyancy effects, which might give rise to convective recirculation of the sampled air stream inside the inlet pipe. For simple flow geometries it is sufficient to estimate the effects of buoyancy using the buoyancy parameter, Gr/Re^2 (Incropera and DeWitt, 1999), which is a dimensionless number that compares the strength of buoyant forces with that of inertial forces using a characteristic length (the tube diameter) and temperature difference (here the difference between wall and gas temperatures). When Gr/Re^2 is smaller than unity, the flow is dominated by inertial forces and buoyancy can be neglected. In case of the main inlet pipe, in which the flow is 11 l min^{-1}, even a temperature difference of 60 °C between the tube wall and the gas would only result in a buoyancy parameter of 0.2. For typical temperature differences of about 10 °C, the buoyancy parameter would be 0.03, so buoyancy inside the main inlet pipe is not important and we can safely neglect it.

The inlet assembly leading to the funnel at the top of the inlet pipe is designed to raise the temperature of the sample from that of the (possibly very cold) ambient outside air to that of the AMS. Since the flow speeds are slowest in this region, the inertial forces are weakest and it is not possible to exclude convective recirculation simply on the basis of the buoyancy parameter, which in this case is larger than unity. Therefore, we have modeled the flow in the inlet assembly using computational fluid dynamics (CFD) (ANSYS CFX; ANSYS 11.0, ANSYS Inc. Canonsburg, PA, USA).

Figure 1 shows the CFD-calculated trajectories of 1 µm diameter particles (density of 1000 kg m^{-3}) that were released across the cross section of the opening at the bottom of the inlet. For this purpose, the air entering the opening was assumed to have a temperature of −40 °C. The CFD analysis shows that buoyant forces cause the air and particles to rise faster in the proximity of the heated walls than in the other parts of the

ACPD
10, 13407–13443, 2010

inlet. This draws the particles closer to the heated wall, enhancing the heat transfer to them and directing them to the region above the inlet pipe, from which they are swept into the top of the funnel. The air in the central region of the gap between the inlet pipe and the heated can is nearly stagnant. The slow circulation there does not affect particles in the size range detectable by the AMS (approximately 80 nm to 700 nm). Particles larger than about 25 µm (aerodynamic diameter) are eliminated in the inlet by elutriation (they are too heavy and are not carried up into the inlet), while particles with diameters of 10 µm or smaller have transmission efficiency through the inlet region of 100%.

The CFD results also verified the effective heating of air in the inlet. The air inside the funnel reaches a temperature ≥15 °C when the sampled air is at −40 °C if the inlet wall is kept at 20 °C. Of course, the particles are very well coupled thermally to the air under the conditions of our inlet, so are heated to the same temperature.

After entering the inlet pipe, the air flows through three 90° bends before being sampled by the AMS: the first is a Swagelok Tee where 6 l/min is taken from the 11 l min^{-1} inlet flow; the second is a 90° elbow; and the third is another Tee, where 1 l min^{-1} is split from the 6 l min^{-1} flow. At a flow rate of 6 l min^{-1}, losses at a 90° bend in a tube with ID of 22 mm (approximating the first Swagelok Tee) are very close to zero. For particles of 10 µm aerodynamic diameter, the transport efficiency through the bend is 99% (Hinds, 1999). This may also be confirmed directly from the fact that the Stokes numbers in this flow for particles having diameters less than 10 µm are much smaller than unity (approximately 6×10^{-3} and 7×10^{-5} for 10 µm and 1 µm particles respectively). Hence particles smaller than 1 µm, which is above the upper limit for detection by the AMS, will follow the air stream without problems. Similar calculations confirm that losses in the other two bends for particles smaller than 10 µm are also close to zero, a result that was also confirmed using CFD modelling of particle flow through these bends.

Diffusion losses in the sampling line were also evaluated using (Gormley and Kennedy, 1949). The 11 l min^{-1} flow through the 7.2 m long sampling pipe yields a

ACPD
10, 13407–13443, 2010

transmission efficiency of 99.3% for 70 nm particles (below lower detection limit of AMS, which detects particles of about 80 nm with a 50% efficiency, Liu et al., 2007). Transmission efficiencies in the sections having 6 l/min and 1l/min flows are even higher. The 15.5 cm long tube through which the AMS samples with its 80 ml/min flow has the lowest transmission efficiency with 98.6% for 80 nm particles. Overall, the diffusion losses should amount to about 3% for particles with 70 nm diameter and losses for larger particles are smaller.

2.3 Sampling protocol

For the results reported here, the AMS operated continuously using a one-hour signal averaging cycle. The averaged aerosol mass spectrum and size distributions of the selected species in TOF mode are saved each hour and then analyzed using previously-developed methods (Alfarra et al., 2004; Allan et al., 2003a, b, 2004; Jimenez et al., 2003). Calibration procedures are carried out once per week, including adjustment of the electron multiplier voltage and determination of its gain. Calibration of the overall ionization and detection efficiency (IE) (Allan et al., 2003b; Canagaratna et al., 2007; Jimenez et al., 2003) is performed using a narrow size range selected from a polydisperse ammonium nitrate aerosol (Jayne et al., 2000). Our procedure differs slightly from the conventional AMS calibration (Allan et al., 2003b; Canagaratna et al., 2007; Jimenez et al., 2003), which generates the monodisperse test aerosol using a differential mobility analyzer. We use a polydisperse aerosol together with the sizing capability of the AMS, which is calibrated using size certified polystyrene latex spheres (Jayne et al., 2000). Tests performed in the laboratory prior to installation at PEARL showed that our method gave 10 to 15% lower IE values.

ACPD
10, 13407–13443, 2010

3 Results

The mass concentrations of the chemical species were determined from the measured mass spectra using the fragmentation table as described by (Allan et al., 2004). The lower detection limits for these mass concentrations were estimated as three times the standard deviation of the hourly averages during periods with close to zero concentrations (Allan et al., 2003a; Rupakheti et al., 2005). For a period with relatively low and constant concentrations (10 to 11 September 2006), this yielded detection limits of 0.02 $\mu g\,m^{-3}$ for ammonium, 0.002 $\mu g\,m^{-3}$ for nitrate, 0.003 $\mu g\,m^{-3}$ for sulfate, and 0.04 $\mu g\,m^{-3}$ for organics.

Figures 2 and 3 show the time series of AMS mass concentrations of sulfate, total organics, ammonium and nitrate for the aerosol sampled between 5 August 2006 and 12 October 2006, a period with high data coverage (valid data were collected during 97% of the time). The water mass concentration is shown only for particle-bound water (i.e. when water correlates obviously with one of the particulate signals). Thus water signals due to varying air humidity levels are ignored (see below). For this period the average mass concentrations for ammonium, nitrate, sulfate, and organics were 0.02 $\mu g\,m^{-3}$, 0.007 $\mu g\,m^{-3}$, 0.115 $\mu g\,m^{-3}$ and 0.11 $\mu g\,m^{-3}$ respectively. Sulfate was present at concentrations significantly above our previously-defined detection limit. The organics and nitrate concentration were clearly above their detection limit most of the time, while most ammonium measurements were approximately at the detection limit. Therefore the ammonium measurement was determined to be too noisy and was not considered in subsequent analyses.

3.1 Regional atmospheric chemistry

The data recorded during the first months following the AMS installation give information about the local concentrations that is relevant for the interpretation of the episodes that we will describe later in this paper. During the sampling period, it was found that the absolute mass concentrations of ammonium and nitrate were very low (maxima ~

ACPD
10, 13407–13443, 2010

0.03–0.05 µg m^{-3}) whereas those of the organic and sulfate components were much higher (maxima ~0.5 and 1 µg m^{-3} respectively). Ammonium nitrate will only form after all the sulfate has been neutralized, so the high sulfate/ammonium ratios indicate that very little ammonium nitrate was present during the sampling period. There is, however, a good correlation between nitrates and organics that persists through the whole dataset. This suggests strongly that the small nitrate mass concentrations that were observed stem from organic nitrates. In this context, we note that if inorganic nitrate were present, it is possible that it might be partially re-partitioned from the aerosol to the gas phase during transit through the room temperature inlet following sampling from cold ambient conditions. If this occurred, the inorganic component would be underestimated. In view of the discussion at the beginning of this section, however, it is clear that inorganic nitrate aerosol is negligible during the sampling period.

3.2 Correlations

Correlations among the sulfate, organics and nitrates for the period shown in Figs. 2 and 3 give information about possible common origins for some of these species. The overall correlation coefficient between sulfate and organics for this period is R^2=0.38. Closer examination of the scatter plot shown in Fig. 4 for these two species, however, suggests that aerosols from at least two different sources were sampled. During an episode of high sulfate concentrations that lasted two and a half days (61 h, between 1 September 2006 01:00 UTC and 3 September 2006 13:00 UTC; shown in blue in Fig. 4), the measurements show a high correlation between sulfate and organics (R^2=0.64), combined with a slowly-varying organic background of around 0.1 µg m^{-3} (i.e. the positive intercept in Fig. 4). Another subset of measurements with even higher sulfate-to-organics correlation occurred in the data sampled on ten consecutive days between 2 October 2006 and 12 October 2006. These data are shown in green on Fig. 4. In this case the correlation coefficient is R^2=0.80, but there is no significant intercept, suggesting that both particulate organics and sulfate (possibly as precursor

ACPD
10, 13407–13443, 2010

gases) arrive from the same source region in a background-free air mass. We will report the results of Lagrangian studies of these two episodes later in this paper. For other time periods the correlation coefficients are much lower (e.g. R^2=0.06 for 3–11 September 2006). Although there are episodes of both high organic and sulfate particle concentrations during this period, the lack of correlation indicates that they come from different sources and/or geographic regions.

The overall sulfate-nitrate correlation during the same period (5 August 2006 to 12 October 2006) is also weak, with R^2=0.24, but the scatter plot shown in Fig. 5, reveals periods of higher correlation having similar structures to that of the sulfate-organics episode. These correspond roughly to the two groups of data with higher correlations shown in Fig. 4. Data from the first group (high sulfate ($SO_4^=$) episode between 1 September 2006 01:00 UTC and 3 September 20060 13:00 UTC) approximately coincide with the points having $SO_4^=$ concentrations above 0.5 µg m^{-3} in Fig. 5. These data follow a different trend than points with SO_4 below about 0.4 µg m^{-3}. The second group of data between 2 October 2006 and 12 October 2006 (shown in green on the scatter plot of Fig. 5) have sulfate concentrations below 0.4 µg m^{-3} and a correlation coefficient R^2=0.50.

The correlation between nitrate and organics, which is shown in Fig. 6, has a higher overall R^2 value of 0.45. This correlation is consistent throughout the entire two months period studied, and no shorter episodes with significantly higher or lower correlation could be identified. This rough correlation between the nitrates and organics in the air at PEARL combined with the absence of natural sources for nitrates near the PEARL laboratory, suggests that both stem from air that is transported to PEARL from low latitude sources where nitrates are prevalent. Since there are no identifiable episodes of very high nitrate concentrations that would indicate localised sources, it is likely that the sources are geographically widespread. This is consistent with agricultural activity as the most likely source, as is the time period, which corresponds to the fall application of nitrate fertilizer. We will comment further on this in the section that reports the Lagrangian calculations.

ACPD
10, 13407–13443, 2010

Relatively low ratios of NO_2^+:NO^+ (below 0.5 most of the time and approximately 0.2 on average) are a further indication that organic nitrate aerosol accounts for most of the measured nitrate (Fry et al., 2009). During calibration of the AMS with ammonium nitrate this ratio is around 1. These organic nitrates are most likely formed during transport and are responsible for the observed good correlation between nitrate and organics. This would also explain the different sulfate-nitrate trend that we pointed out above for data with sulfate concentrations higher than 0.5 µg m^{-3}. These data were measured during an exceptionally high sulfate episode around 2 September 2006 that was accompanied by a modest increase in the concentration of organics (see Fig. 2). The organic aerosol, however, remained correlated to nitrate during the entire episode.

While it is possible that sulfur might have been present in form of ammonium sulfate or bisulfate during periods of low sulfate concentrations, the very low ammonium levels are inconsistent with these compounds being present during episodes with higher sulfur concentrations. This differs from typical urban environments, where most of the sulfur is present as ammonium sulfate and during shorter episodes of increased acidity, ammonium bisulfate is present as well (e.g. Zhang et al., 2005). This suggests that the sulfate aerosol detected during these episodes is probably very highly oxidized and is thus predominantly in the form of sulfuric acid.

3.3 Size distributions

Mass size distributions of the major chemical species are derived from the AMS measurements in TOF mode (Jimenez et al., 2003). The TOF size distributions shown in Fig. 7 are averaged over 21 September 2006 to 2 October 2006, a period that had above average sulfate and organics mass concentrations. The size distributions have been normalized to the mass concentrations determined from measurements in the MS mode (Allan et al., 2003a; as described in Allan et al., 2003b). The sulfate has a distribution between (vacuum aerodynamic) diameters of approximately 200 and 700 nm. The large diameter cutoff may be due in part to the reduced transmission efficiency of the AMS inlet system above this size (Jayne et al., 2000), because Liu

ACPD
10, 13407–13443, 2010

et al. (2007) have shown that the transmission efficiency for particles of various compositions drops to about 50% at around 700 nm. The sulfate distribution is very broad and the shape suggests that it might consist of two modes, one with maximum at approximately 300 nm and one at about 500 nm (or larger). The maximum in the organic aerosol size distribution is at about 350 nm. A weak nitrate mode is also evident in this size range.

Figure 8 shows the size distribution for the short period with exceptionally high sulfate concentration between 1 September 2006 01:00 UTC and 2 September 2006 19:00 UTC (average sulfate concentration of 0.79 $\mu g\,m^{-3}$). The sulfate mode has a maximum at approximately 500 nm; the maximum in the organic mode is at 450 nm. No significant nitrate was observed during this period. There is, however, a high concentration of particle-bound water (i.e. water that was not evaporated from the particle before detection by the AMS). This can be seen in both the time series of total mass concentration and the TOF size distributions. Water that is evaporated from cloud or fog particles in the inlet is seen as fluctuations that have no correlation with the other components. In this case, however, the water signal showed a relatively high correlation with the sulfate (R^2=0.46 in MS mode), whereas this R^2 value was 0.07 on the two days prior to this episode. Moreover, the water and sulfate have nearly identical mass size distributions as shown in Fig. 8, strongly suggesting that the water was contained in the sulfate particles and was not removed when these particles were heated to room temperature.

During all other periods no identifiable TOF water mode can be distinguished, even on those occasions when the mass concentration of water correlates with sulfate or organics. The absence of a water TOF mode means that little or no moisture remains in the detected particles after passage through the sampling system, indicating that the sampled particles were either dry on entry or contained at most a surface layer of water that evaporates easily. This is consistent with the fact that the temperatures in the vicinity of Eureka were about −12 °C during the sampling period and thus the relative humidity of the air would have been very low after raising its temperature to

ACPD
10, 13407–13443, 2010

20°C in the inlet. Since the water was not evaporated during the high sulfate episode discussed above, therefore, we conclude that both the sulfate and water come from condensed sulfuric acid. The small amount of organic material present with the water and sulfate might be from organic aerosols coated with sulfuric acid or from separate organic particles that coincidentally have the same size distribution (Heintzenberg and Leck, 1994). The former, however, seems more likely (Nriagu et al., 1991).

All mass size distributions measured by the AMS during the two months analyzed here extend from about 200 or 300 nm to the upper limit of the AMS at about 700 nm. Although the lower detection limit of the AMS (given at 50% efficiency) is at 80 nm (Liu et al., 2007), none of the measured size distributions show particles below about 200 nm. The absence of ultrafine or Aitken mode particles shows there is no particle formation in the vicinity of PEARL; the arriving particles are aged and thus originate from distant sources. This may be contrasted with AMS studies in urban environments, which usually show two modes: one at 100–200 nm and a larger one between 300 and 800 nm. The smaller mode is normally identified as newly-formed organic particles originating (usually) from motor vehicle emissions, whereas the larger consists of sulfate, nitrate, and oxidized organics (Alfarra et al., 2004; Allan et al., 2003a; Rupakheti et al., 2005). The absence of the smaller mode at PEARL is consistent with results from rural regions, where smaller modes are usually not observed (Alfarra et al., 2004; Rupakheti et al., 2005).

4 Lagrangian modelling

The correlations described in the last section for some of the episodes are suggestive of common origins, so these episodes were chosen for source identification using the Lagrangian particle dispersion model FLEXPART (Stohl et al., 1998; Stohl and Thomson, 1999). FLEXPART simulates the long-range transport, diffusion, wet and dry deposition, and radioactive decay of tracers released from point, line, area or volume sources. It can be run either in the forward mode to simulate the dispersion of tracers

ACPD
10, 13407–13443, 2010

from their sources, or backward in time to determine potential source contributions to a specified receptor. FLEXPART has been extensively validated with data from large-scale tracer experiments in North America and Europe (Stohl et al., 1998) and used in many other atmospheric transport studies. Of relevance to the present high latitude application, FLEXPART was used recently to simulate the transport of pollutant plumes from Russian (Damoah et al., 2004) and Alaskan (Damoah et al., 2006) forest fires. For the simulations reported here, FLEXPART was driven by meteorological data from the Global Forecast System (GFS) of the National Center for Environmental Prediction using a horizontal resolution of 1°×1° with 26 pressure levels and a time resolution of 3 h (analyses at 00:00, 06:00, 12:00, 18:00 UTC; 3-h forecasts at 03:00, 09:00, 15:00, 21:00 UTC).

Backward simulations were initiated in order to understand the transport mechanisms as well as the origin of the air arriving at PEARL during the episodes described in the preceding sections. The backward simulation employed here is similar to that described by (Siebert, 2001) and (Stohl et al., 2003). We released 20 000 particles at the PEARL receptor location during the episode periods and simulated their transport backward in time for 20 days, forming a "retroplume". We then computed particle residence times in seconds, normalized by the total number of released particles, in the cells of a 3-D grid with 1°×1° horizontal resolution and 500 m vertical depth, for each 3 h transport period.

The residence time in the grid boxes near the surface (called the source "footprint", see Flesch et al. (1995) is proportional to the contribution a source of unit strength located in those grid boxes, would make to the mixing ratio at the receptor. If the absolute contributions from the grid boxes are required in terms of mass concentrations for a particular species, then we multiply the residence times in the grid boxes with the source strength of that species. For the sulfate episode, we used the SO_2 emission for the year 2000 from the Emission Database for Global Atmospheric Research (EDGAR) v3.2 (Olivier et al., 2005) as a proxy for the detected sulfate, on the assumption that the SO_2 would be completely oxidized during transport over the long distances from most

ACPD
10, 13407–13443, 2010

sources.

4.1 Lagrangian results

The first period chosen for source identification is from 30 August to 3 September, 2006, when the AMS recorded sulfate concentrations more than 5 times higher than the average background. Organic concentrations were also enhanced substantially during this period and we will analyse this and other organic episodes in a future report. For the present purposes, however, we will focus on the sulfate results. The episode shown in Fig. 2 has two identifiable parts: a small one from 30 August 2006 at 00:00 UTC to 31 August 2006 at 00:00 UTC and a second, much larger one from 1 September 2006 at 00:00 UTC to 3 September 2006 at 00:00 UTC. Separate FLEXPART backward simulations were performed for both. For comparison, we also made a model run for particles arriving during 20 August 2006 at 00:00 UTC to 23 August 2006 at 21:00 UTC, where a low background sulfate concentration (i.e. clean air) was observed.

The results from the FLEXPART simulations are shown in Figs. 9–11. The upper panels in each case show the footprint residence time distributions (normalized by the longest residence time) derived from the backward simulations for particles arriving at PEARL during the respective time periods from 20–23 August (Fig. 9, clean air); 30–31 August (Fig. 10; first sulfate episode) and 1–3 September (Fig. 11; second sulfate episode).

For the clean air simulation (Fig. 9), the retroplume footprint is concentrated at high latitudes where anthropogenic SO_2 emissions are nearly zero. The retroplume from both of the other episodes, however, approaches the surface at lower latitudes than that of the clean air case. For the sulfate episode of 30–31 August (Fig. 10), the longest footprint residence times are located over Greenland and extend southwards over the Atlantic Ocean, the north-eastern United States and eastern Canada, as well as significant areas distributed over Russia. For the episode of 1–3 September (Fig. 11), the footprint extends over Alaska through the Arctic Ocean to Asia. In this case the largest residence times are distributed in two parts of Russia: one in the extreme east; the

ACPD
10, 13407–13443, 2010

other in the west.

To obtain the actual source contributions to the mixing ratios at the receptor, we multiply the footprint residence times with the SO_2 emission strengths from the EDGAR inventory. The resulting source contributions (lower panels of Figs. 9, 10 and 11) show the results. For the clean air period, the source map in the lower panel of Fig. 9 shows almost no ($<10^{-6}$ ppbv) sulfate contributions to the mixing ratio at PEARL from anthropogenic SO_2 emissions anywhere in the hemisphere. Combining the EDGAR emission data with the footprint at the top of Fig. 10 shows that the major source contributions to the pollution episode of 30–31 August are located in the north eastern United States and eastern Canada (blue rectangle), with significant contributions as well from central and western Russia (red rectangle). For the later episode recorded on 1–3 September, the west-central Russian region (red rectangle in Fig. 11) is seen to be the most important source contributor with again some smaller contributions distributed over eastern Russia. The EDGAR SO_2 emission data show that the former is a particularly strong anthropogenic SO_2 emission region.

The source regions shown by the red and blue rectangles in Figs. 10 and 11 coincide with the locations where anthropogenic sulfate emissions could be expected. The North American footprint includes the largest population densities in eastern United States and central Canada, including the Washington-Baltimore-Philadelphia-New York urban region, and the Greater Toronto Area. The highest concentration of emissions in Fig. 11 coincides with the oil and gas fields of western Siberia, which produce approximately 9.8 Mbbl of oil per day, of which, about 30% is refined locally (US EIA, 2009). Total oil refinery throughput in Russia is about 4.6 Mbbl/d, but the recovery efficiency is low due to aging equipment, so losses to the atmosphere are larger than occur with more modern equipment. It is also possible that the more widely distributed source regions in eastern Russia contribute to the sulfate detected at PEARL, but the short temporal span of the episode argues for a more compact source such as that in western Russia. These regions are being investigated in greater detail using slightly different tracer techniques. We hope to report the results of this work soon.

ACPD
10, 13407–13443, 2010

5 Conclusions

We have described the installation of an AMS at the PEARL observatory in the Canadian high Arctic and discussed several aspects of the installation that ensure the integrity of particles sampled from the very cold and harsh environment at the laboratory. The unique remote location of the laboratory at 80° N and an altitude of 610 m above sea level in the free troposphere make it an ideal site to study the long range transport of pollutants into the Arctic.

Since its installation, the AMS has been providing a record of the mass concentrations as well as the chemical composition and size distribution of ambient aerosol at the PEARL site. In this paper, we have reported the components and size distributions obtained during several unusual episodes as well as some periods in which normal background was observed. We have identified common origins for some of these components from temporal correlations among their mass concentrations. We have also located specific source regions for selected episodes of high sulfate concentrations using Lagrangian modelling methods. We found that there are two possible source regions for the short episode of 30–31 August. One is located in north-eastern North America in a region of high population density and the other is broadly distributed in central and western Russia. The short duration of this episode argues for a single, geographically compact source, but it is not possible to identify it more precisely on the basis of these data. The source region for the second and stronger episode, which lasted from 1 to 3 September, is located in western Siberia, coinciding with the location of the largest Russian oil and gas fields. In this case, the SO_2 source is almost certainly the operations associated with oil and gas extraction and processing. These observations show that the Arctic is the destination for significant amounts of pollution from high- and mid-latitude industrial and resource activity. The quantification of this transport is very important to our understanding of the sources for Arctic pollution and to international discussions aimed at its abatement. In future publications, we will discuss the sources for other kinds of aerosols, including organics, and compile a climatology

ACPD
10, 13407–13443, 2010

for the transport of these materials into the Arctic.

Acknowledgements. We are grateful for the financial assistance of the Canada Foundation for Climate and Atmospheric Studies (CFCAS) and for helpful discussions with John Jayne, Aerodyne Inc.

References

Alfarra, M. R., Coe, H., Allan, J. D., Bower, K. N., Boudries, H., Canagaratna, M. R., Jimenez, J. L., Jayne, J. T., Garforth, A. A., Li, S. M., and Worsnop, D. R.: Characterization of urban and rural organic particulate in the lower Fraser valley using two Aerodyne aerosol mass spectrometers, Atmos. Environ., 38, 5745–5758, 2004.

Allan, J. D., Alfarra, M. R., Bower, K. N., Williams, P. I., Gallagher, M. W., Jimenez, J. L., McDonald, A. G., Nemitz, E., Canagaratna, M. R., Jayne, J. T., Coe, H., and Worsnop, D. R.: Quantitative sampling using an Aerodyne aerosol mass spectrometer - 2. measurements of fine particulate chemical composition in two UK cities, J. Geophys. Res.-Atmos., 108, 4091, doi:10.1029/2003JD001608, 2003a.

Allan, J. D., Delia, A. E., Coe, H., Bower, K. N., Alfarra, M. R., Jimenez, J. L., Middlebrook, A. M., Drewnick, F., Onasch, T. B., Canagaratna, M. R., Jayne, J. T., and Worsnop, D. R.: A generalised method for the extraction of chemically resolved mass spectra from Aerodyne aerosol mass spectrometer data, J. Aerosol Sci., 35, 909–922, 2004.

Allan, J. D., Jimenez, J. L., Williams, P. I., Alfarra, M. R., Bower, K. N., Jayne, J. T., Coe, H., and Worsnop, D. R.: Quantitative sampling using an Aerodyne aerosol mass spectrometer – 1. techniques of data interpretation and error analysis, J. Geophys. Res.-Atmos., 108, 4090, doi:10.1029/2003JD001607, 2003b.

AMAP: amap assessment 2002: The influence of global change on contaminant pathways to, within, and from the Arctic, 2003.

Bailey, R., Barrie, L. A., Halsall, C. J., Fellin, P., and Muir, D. C. G.: Atmospheric organochlorine pesticides in the western Canadian Arctic: evidence of transpacific transport, J. Geophys. Res.-Atmos., 105, 11805–11811, 2000.

Barrie, L. A., Staebler, R., Toom, D., Georgi, B., Denhartog, G., Landsberger, S., and Wu, D.: Arctic aerosol size-segregated chemical observations in relation to ozone depletion during polar sunrise experiment 1992, J. Geophys. Res.-Atmos., 99, 25439–25451, 1994.

ACPD

10, 13407–13443, 2010

Canagaratna, M. R., Jayne, J. T., Jimenez, J. L., Allan, J. D., Alfarra, M. R., Zhang, Q., Onasch, T. B., Drewnick, F., Coe, H., Middlebrook, A., Delia, A., Williams, L. R., Trimborn, A. M., Northway, M. J., DeCarlo, P. F., Kolb, C. E., Davidovits, P., and Worsnop, D. R.: Chemical and microphysical characterization of ambient aerosols with the aerodyne aerosol mass spectrometer, Mass Spectrom. Rev., 26, 185–222, 2007.

Covert, D. S. and Heintzenberg, J.: Size distributions and chemical-properties of aerosol at Ny Ålesund, Svalbard, Atmos. Environ. A, 27, 2989–2997, 1993.

Damoah, R., Spichtinger, N., Forster, C., James, P., Mattis, I., Wandinger, U., Beirle, S., Wagner, T., and Stohl, A.: Around the world in 17 days - hemispheric-scale transport of forest fire smoke from Russia in May 2003, Atmos. Chem. Phys., 4, 1311–1321, doi:10.5194/acp-4-1311-2004, 2004.

Damoah, R., Spichtinger, N., Servranckx, R., Fromm, M., Eloranta, E. W., Razenkov, I. A., James, P., Shulski, M., Forster, C., and Stohl, A.: A case study of pyro-convection using transport model and remote sensing data, Atmos. Chem. Phys., 6, 173–185, doi:10.5194/acp-6-173-2006, 2006.

Flesch, T. K., Wilson, J. D., and Yee, E.: Backward-time lagrangian stochastic dispersion models and their application to estimate gaseous emissions, J. Appl. Meteorol., 34, 1320–1332, 1995.

Fry, J. L., Kiendler-Scharr, A., Rollins, A. W., Wooldridge, P. J., Brown, S. S., Fuchs, H., Dubé, W., Mensah, A., dal Maso, M., Tillmann, R., Dorn, H.-P., Brauers, T., and Cohen, R. C.: Organic nitrate and secondary organic aerosol yield from NO_3 oxidation of β-pinene evaluated using a gas-phase kinetics/aerosol partitioning model, Atmos. Chem. Phys., 9, 1431–1449, doi:10.5194/acp-9-1431-2009, 2009.

Gormley, P. G. and Kennedy, M.: Diffusion from a stream flowing through a cylindrical tube, Proceedings of the Royal Irish Academy, A52, 163-169, 1949.

Halsall, C. J., Bailey, R., Stern, G. A., Barrie, L. A., Fellin, P., Muir, D. C. G., Rosenberg, B., Rovinsky, F. Y., Kononov, E. Y., and Pastukhov, B.: Multi-year observations of organohalogen pesticides in the Arctic atmosphere, Environ. Pollut., 102, 51–62, 1998.

Halsall, C. J., Barrie, L. A., Fellin, P., Muir, D. C. G., Billeck, B. N., Lockhart, L., Rovinsky, F. Y., Kononov, E. Y., and Pastukhov, B.: Spatial and temporal variation of polycyclic aromatic hydrocarbons in the Arctic atmosphere, Environ. Sci. Technol., 31, 3593–3599, 1997.

Heidam, N. Z., Wahlin, P., and Kemp, K.: Arctic aerosols in Greenland, Atmos. Environ. A, 27, 3029–3036, 1993.

ACPD
10, 13407–13443, 2010

Heintzenberg, J.: Arctic haze – air-pollution in polar-regions, Ambio, 18, 50–55, 1989.
Heintzenberg, J. and Leck, C.: Seasonal-variation of the atmospheric aerosol near the top of the marine boundary-layer over Spitsbergen related to the Arctic sulfur cycle, Tellus B, 46, 52–67, 1994.
Hillamo, R., Kerminen, V. M., Aurela, M., Makela, T., Maenhaut, W., and Leck, C.: Modal structure of chemical mass size distribution in the high Arctic aerosol, J. Geophys. Res.-Atmos., 106, 27555–27571, 2001.
Hinds, W. C.: Aerosol Technology: Properties, Behavior, and Measurement of Airborne Particles, John Wiley & Sons, New York, 1999.
Hoff, R. M., Leaitch, W. R., Fellin, P., and Barrie, L. A.: Mass size distributions of chemical-constituents of the winter Arctic aerosol, J. Geophys. Res.-Oceans and Atmos., 88, 947–956, 1983.
Hung, H., Blanchard, P., Halsall, C. J., Bidleman, T. F., Stern, G. A., Fellin, P., Muir, D. C. G., Barrie, L. A., Jantunen, L. M., Helm, P. A., Ma, J., and Konoplev, A.: Temporal and spatial variabilities of atmospheric polychlorinated biphenyls (PCBs), organochlorine (OC) pesticides and polycyclic aromatic hydrocarbons (PAHs) in the Canadian Arctic: results from a decade of monitoring, Sci. Total Environ., 342, 119–144, 2005.
Incropera, F. P. and DeWitt, D. P.: Fundamentals of Heat and Mass Transfer, Wiley, New York, 1999.
Jayne, J. T., Leard, D. C., Zhang, X. F., Davidovits, P., Smith, K. A., Kolb, C. E., and Worsnop, D. R.: Development of an aerosol mass spectrometer for size and composition analysis of submicron particles, Aerosol Sci. Technol., 33, 49–70, 2000.
Jimenez, J. L., Jayne, J. T., Shi, Q., Kolb, C. E., Worsnop, D. R., Yourshaw, I., Seinfeld, J. H., Flagan, R. C., Zhang, X. F., Smith, K. A., Morris, J. W., and Davidovits, P.: Ambient aerosol sampling using the Aerodyne Aerosol Mass Spectrometer, J. Geophys. Res.-Atmos., 108(D7), 8425, doi:10.1029/2001JD001213, 2003.
Lammel, G., Sehili, A. M., Bond, T. C., Feichter, J., and Grassl, H.: Gas/particle partitioning and global distribution of polycyclic aromatic hydrocarbons – a modelling approach, Chemosphere, 76, 98–106, 2009.
Liu, P. S. K., Deng, R., Smith, K. A., Williams, L. R., Jayne, J. T., Canagaratna, M. R., Moore, K., Onasch, T. B., Worsnop, D. R., and Deshler, T.: transmission efficiency of an aerodynamic focusing lens system: Comparison of model calculations and laboratory measurements for the aerodyne aerosol mass spectrometer, Aerosol Sci. Technol., 41, 721–733, 2007.

ACPD
10, 13407–13443, 2010

Narukawa, M., Kawamura, K., Li, S. M., and Bottenheim, J. W.: Dicarboxylic acids in the Arctic aerosols and snowpacks collected during Alert 2000, Atmos. Environ., 36, 2491–2499, 2002.
Nriagu, J. O., Coker, R. D., and Barrie, L. A.: Origin of sulfur in Canadian Arctic haze from isotope measurements, Nature, 349, 142–145, 1991.
Nyeki, S., Coulson, G., Colbeck, I., Eleftheriadis, K., Baltensperger, U., and Beine, H. J.: Overview of aerosol microphysics at Arctic sunrise: measurements during the NICE renoxification study, Tellus B, 57, 40–50, 2005.
Oehme, M.: Further evidence for long-range air transport of polychlorinated aromates and pesticides – North America and Eurasia to the Arctic, Ambio, 20, 293–297, 1991.
Oehme, M. and Ottar, B.: The long-range transport of polychlorinated hydrocarbons to the Arctic, Geophys. Res. Lett., 11, 1133–1136, 1984.
Olivier, J. G. J., Van Ardenne, J. A., Dentner, F., Ganzeveld, L., and Peters, J. A. H.: Recent trends in global greenhouse gas emissions regional trends and spatial distribution of key sources, 325–330, in: Air pollution Modeling and its Application XI; Proceedings of ITM Boulder, edited by: Gryning, S. E. and Schiermeier, F. A., Plenum, New York, 2001.
Pacyna, J. M.: The origin of Arctic air-pollutants – lessons learned and future-research, Sci. Total Environ., 161, 39–53, 1995.
Polissar, A. V., Hopke, P. K., and Harris, J. M.: Source regions for atmospheric aerosol measured at barrow, alaska, Environ. Sci. Technol., 35, 4214–4226, 2001.
Ricard, V., Jaffrezo, J. L., Kerminen, V. M., Hillamo, R. E., Teinila, K., and Maenhaut, W.: Size distributions and modal parameters of aerosol constituents in northern finland during the european Arctic aerosol study, J. Geophys. Res.-Atmos., 107, 4370, doi:10.1029/2002JD002862, 2002.
Rupakheti, M., Leaitch, W. R., Lohmann, U., Hayden, K., Brickell, P., Lu, G., Li, S. M., Toom-Sauntry, D., Bottenheim, J. W., Brook, J. R., Vet, R., Jayne, J. T., and Worsnop, D. R.: An intensive study of the size and composition of submicron atmospheric aerosols at a rural site in ontario, canada, Aerosol Sci. Technol., 39, 722–736, 2005.
Saarikoski, S., Timonen, H., Saarnio, K., Aurela, M., Järvi, L., Keronen, P., Kerminen, V.-M., and Hillamo, R.: Sources of organic carbon in fine particulate matter in northern European urban air, Atmos. Chem. Phys., 8, 6281–6295, doi:10.5194/acp-8-6281-2008, 2008.
Sehili, A. M. and Lammel, G.: Global fate and distribution of polycyclic aromatic hydrocarbons emitted from europe and russia, Atmos. Environ., 41, 8301–8315, 2007.

ACPD
10, 13407–13443, 2010

Siebert, P.: Inverse modeling with a lagrangian particle dispersion model, application to point releases over limited time intervals, in: Air pollution Modeling and its Application XI; Proceedings of ITM Boulder, edited by: Gryning, S. E. and Schiermeier, F. A., Plenum, New York, 381–389, 2001.

Sirois, A. and Barrie, L. A.: Arctic lower tropospheric aerosol trends and composition at Alert, canada: 1980–1995, J. Geophys. Res.-Atmos., 104, 11599–11618, 1999.

Staebler, R., Toom-Sauntry, D., Barrie, L., Langendorfer, U., Lehrer, E., Li, S. M., and Dryfhout-Clark, H.: Physical and chemical characteristics of aerosols at spitsbergen in the spring of 1996, J. Geophys. Res.-Atmos., 104, 5515–5529, 1999.

Stohl, A., Forster, C., Eckhardt, S., Spichtinger, N., Huntrieser, H., Heland, J., Schlager, H., Wilhelm, S., Arnold, F., and Cooper, O.: A backward modeling study of intercontinental pollution transport using aircraft measurements, J. Geophys. Res.-Atmos., 108, 4370, doi:10.1029/2002JD002862, 2003.

Stohl, A., Hittenberger, M., and Wotawa, G.: Validation of the lagrangian particle dispersion model flexpart against large-scale tracer experiment data, Atmos. Environ., 32, 4245–4264, 1998.

Stohl, A. and Thomson, D. J.: A density correction for lagrangian particle dispersion models, Bound.-Lay. Meteorol., 90, 155–167, 1999.

Ström, J., Umegard, J., Torseth, K., Tunved, P., Hansson, H. C., Holmen, K., Wismann, V., Herber, A., and Konig-Langlo, G.: One year of particle size distribution and aerosol chemical composition measurements at the Zeppelin station, Svalbard, March 2000–March 2001, Phy. Chem. Earth, 28, 1181–1190, 2003.

Teinilä, K., Hillamo, R., Kerminen, V. M., and Beine, H. J.: Chemistry and modal parameters of major ionic aerosol components during the NICE campaigns at two altitudes, Atmos. Environ., 38, 1481–1490, 2004.

Teinilä, K., Hillamo, R., Kerminen, V. M., and Beine, H. J.: Aerosol chemistry during the NICE dark and light campaigns, Atmos. Environ., 37, 563–575, 2003.

US EIA: Russian Oil Production, online available at: http://www.eia.doe.gov/emeu/cabs/Russia/Background.html, last accessed 21 May 2010.

Xie, Y. L., Hopke, P. K., Paatero, P., Barrie, L. A., and Li, S. M.: Locations and preferred pathways of possible sources of Arctic aerosol, Atmos. Environ., 33, 2229–2239, 1999.

Zhang, Q., Canagaratna, M. R., Jayne, J. T., Worsnop, D. R., and Jimenez, J. L.: Time- and size-resolved chemical composition of submicron particles in Pittsburgh: im-

ACPD
10, 13407–13443, 2010

plications for aerosol sources and processes, J. Geophys. Res.-Atmos., 110, D07S09, doi:10.1029/2004JD004649, 2005.

ACPD
10, 13407–13443, 2010

Fig. 1. A 30° radial section is used to model the flow through the inlet assembly with CFD. Air at −40 °C and 1 µm diameter particles (density of 1000 kg m^{-3}) are introduced through the opening at the bottom of the inlet. The outer surface and the inlet pipe in the center (ending in a funnel at the top) are heated to 20 °C. Trajectories of the 1 µm particles are depicted as grey lines.

ACPD
10, 13407–13443, 2010

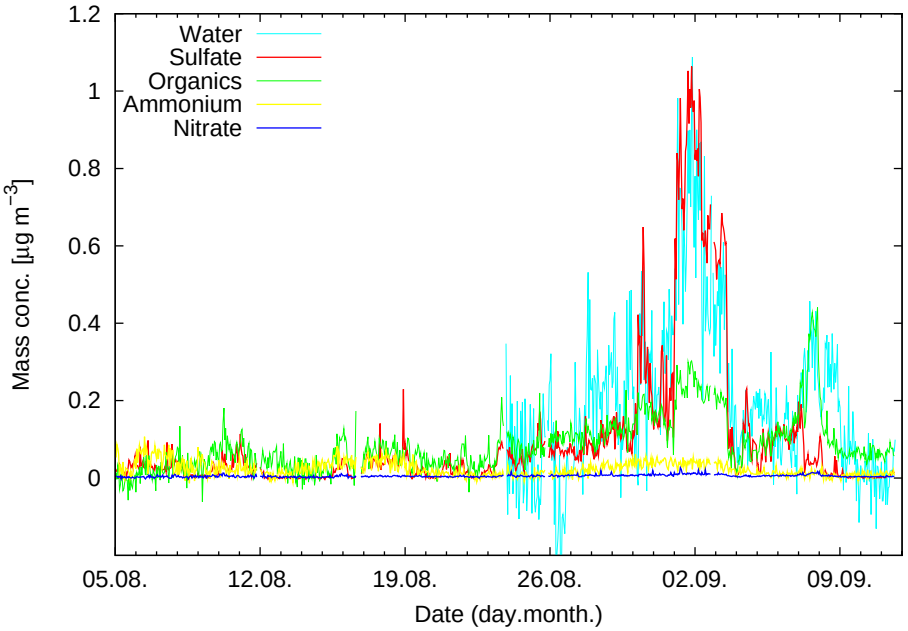

Fig. 2. Time series of AMS mass concentrations of sulfate, total organics, ammonium and nitrate for the aerosol sampled between 5 August 2006 and 11 September 2006.

ACPD
10, 13407–13443, 2010

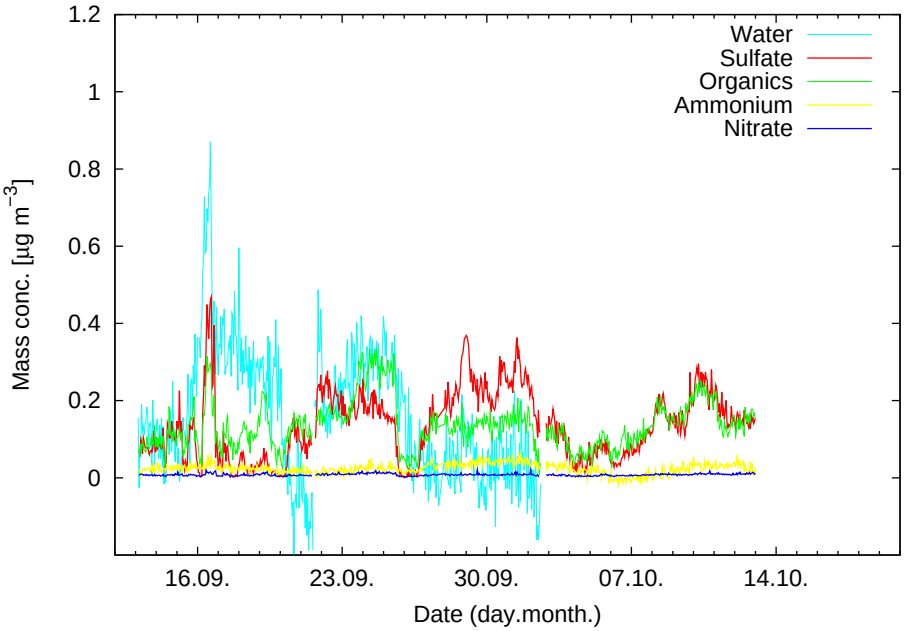

Fig. 3. Time series of AMS mass concentrations of sulfate, total organics, ammonium and nitrate for the aerosol sampled between 13 September 2006 and 12 October 2006.

ACPD
10, 13407–13443, 2010

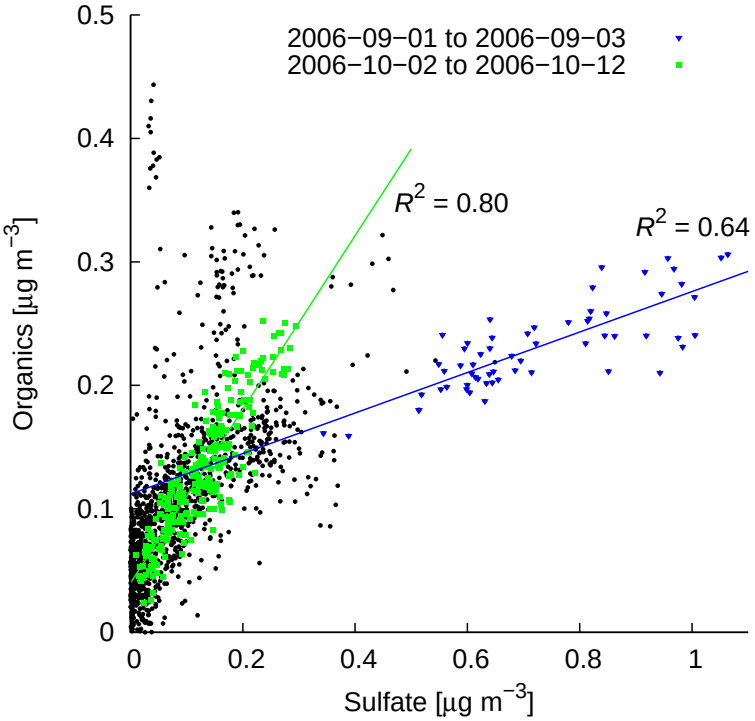

Fig. 4. Scatter plot of organics and sulfate concentrations showing data between 5 August 2006 and 12 October 2006. Two groups with exceptionally high correlations are indicated with blue and green points. The remaining data are shown as black points.

ACPD
10, 13407–13443, 2010

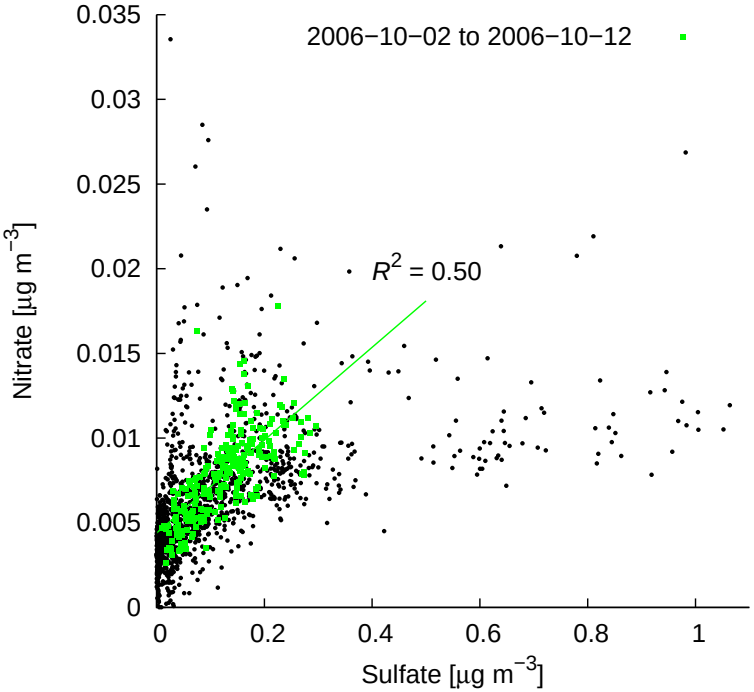

Fig. 5. Scatter plot of nitrate and sulfate concentrations showing data between 5 August 2006 and 12 October 2006. The overall correlation is weak with R^2 of 0.24. One group with high correlation is indicated with green points. The remaining data are shown as black points.

ACPD
10, 13407–13443, 2010

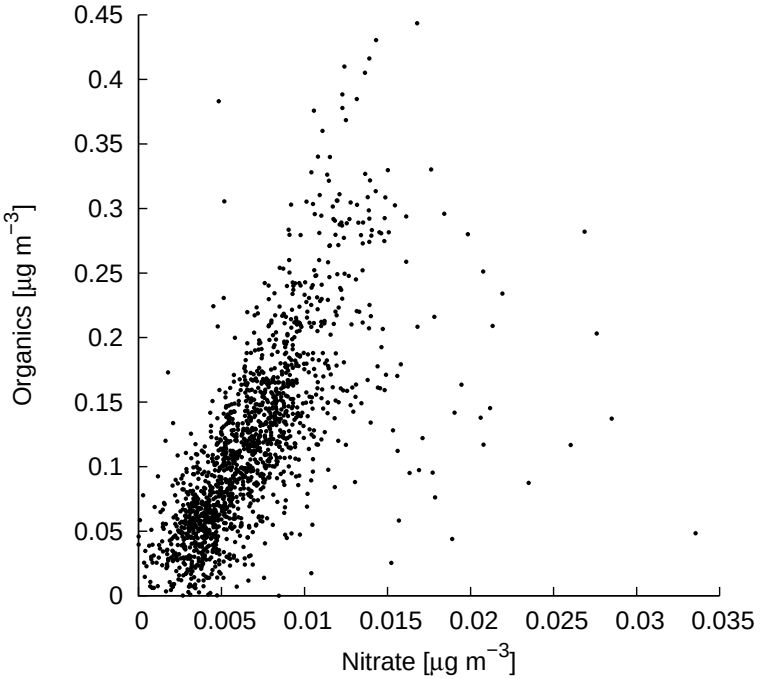

Fig. 6. Scatter plot of organics and nitrate concentrations showing data between 5 August 2006 and 12 October 2006. The consistent overall correlation has an R^2 value of 0.45.

ACPD
10, 13407–13443, 2010

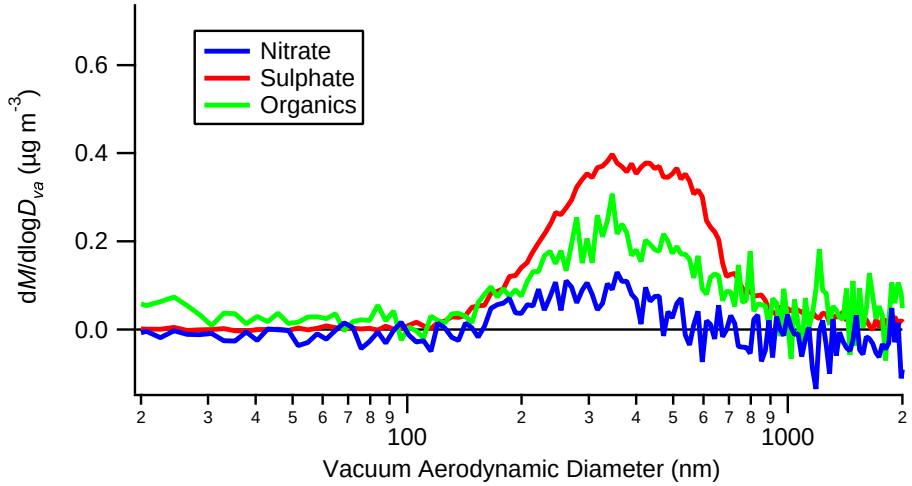

Fig. 7. Mass size distributions averaged over the period from 21 September 2006 to 2 October 2006 having above average sulfate and organics mass concentrations.

ACPD
10, 13407–13443, 2010

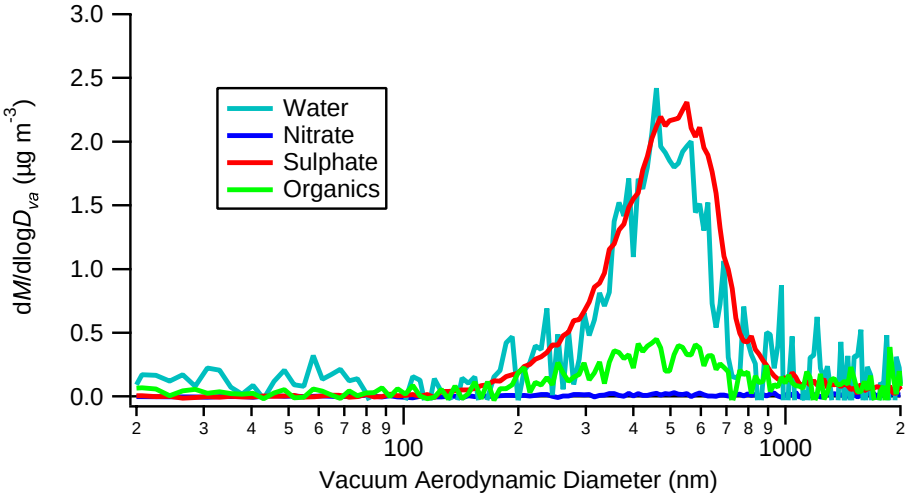

Fig. 8. Mass size distributions for an episode with exceptionally high sulfate concentrations (1 September 2006 01:00 UTC to 2 September 2006 19:00 UTC). During this episode particle-bound water was detected with a size distribution similar to the sulfate size distribution.

ACPD
10, 13407–13443, 2010

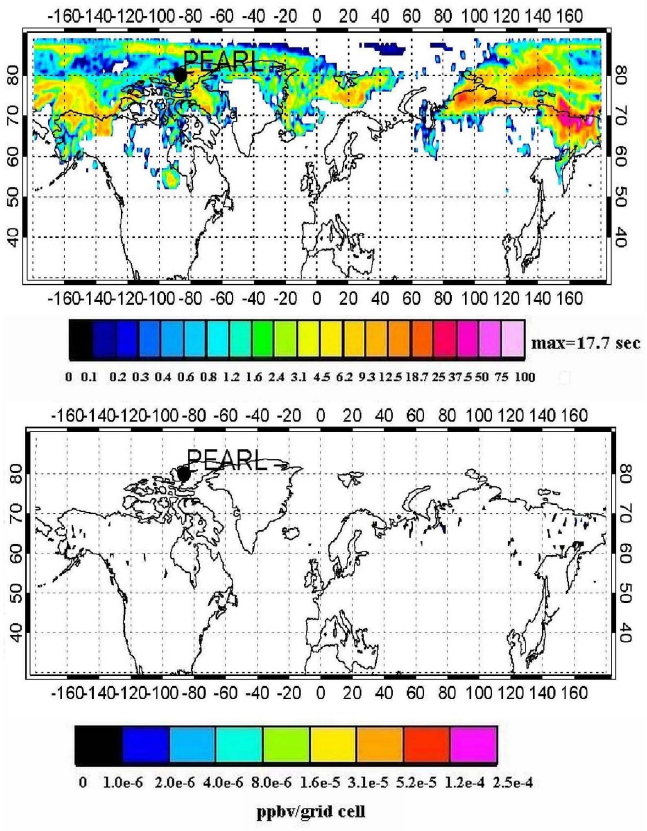

Fig. 9. The top panel shows the footprint residence time distribution for particles arriving at the receptor during the period 26 August 2006 at 00:00 UTC to 29 August 2006 at 21:00 UTC where the AMS recorded low concentrations of sulfate (clean air). The values are expressed as a percentage of the maximum residence time (in seconds) shown under each panel. The corresponding potential source contribution per grid cell to the mixing ratio at the receptor is shown in the bottom panel.

ACPD
10, 13407–13443, 2010

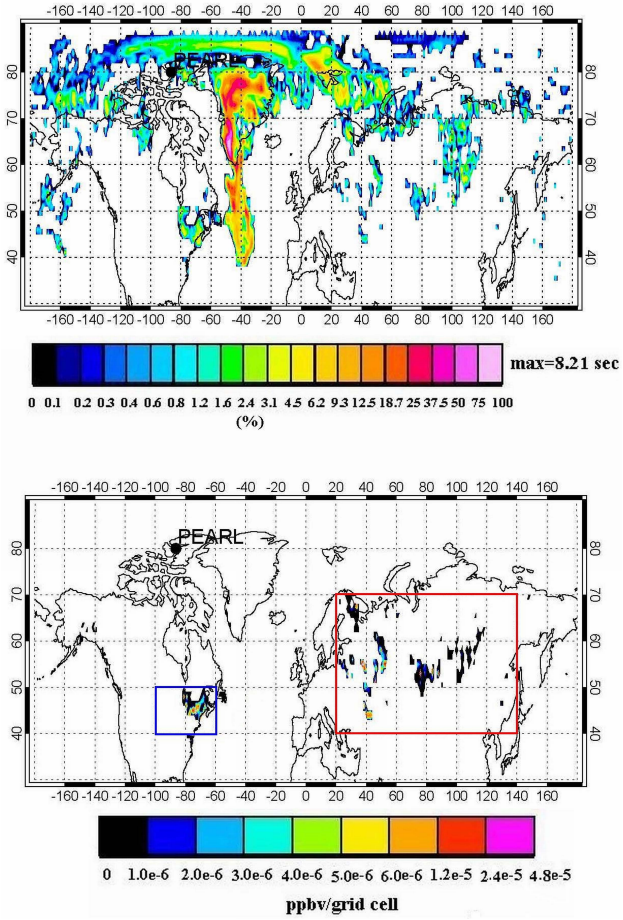

Fig. 10. Similar to Fig. 9 but for particles arriving at the receptor during 30 August 2006 at 00:00 UTC to 31 August 2006 at 00:00 UTC. Predicted regions with strong contributions are indicated by blue and red rectangles.

ACPD
10, 13407–13443, 2010

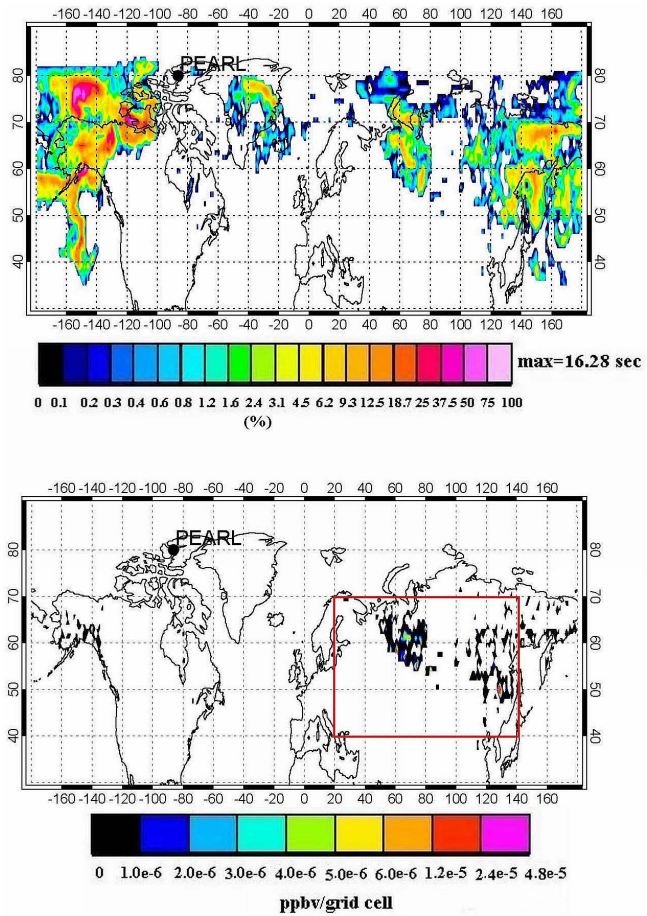

Fig. 11. Similar to Fig. 9 and Fig. 10 but for particles arriving at the receptor during 1 September 2006 at 00:00 UTC to 3 September 2006 at 00:00 UTC.

ACPD
10, 13407–13443, 2010